Chapter 2
Current Problems in the Quasi-elastic Incoherent Neutron Scattering and the Collective Drift of Molecules

Leonid A. Bulavin, N. P. Malomuzh and K. S. Shakun

Abstract The determination of the self-diffusion coefficient D_s is one of well known applications of the quasi-elastic incoherent neutron scattering. Here we will show that the half-width of the neutron peak considered as a function of wave vector can be used for the determination of (1) the residence time τ_0 for water molecules and (2) the very important ratio D_c/D_s where D_c is the collective part of the self-diffusion coefficient, caused by its drift in the field of thermal hydrodynamic fluctuations. The applicability region for the simplest diffusion approximation is discussed in details. The influence of the rotational motion of water molecules on spectra of the intermediate scattering function (ISF) is studied. A new type of the high-frequency asymptote for the ISF-spectra is predicted.

2.1 Introduction

The quasi-elastic incoherent neutron scattering (QEINS) is usually applied for the determination of the self-diffusion coefficient D_s [1–3]. In works [4, 5] it had been shown that the half-width of the neutron peak considered as a function of wave vector can be used for the determination of (1) the residence time τ_0 for water molecules [6–9] and (2) the rotational one τ_r for them. Unfortunately, the magnitude of the last does not correlate with its estimate τ_d following from the dielectric relaxation

L. A. Bulavin
Department of Molecular Physics, Kyiv Taras Shevchenko National University,
2 Academic Glushkov Ave., Kyiv 03680, Ukraine
e-mail: bulavin221@gmail.com

N. P. Malomuzh
Department of Theoretical Physics, Odessa I.I.Mechnikov National University,
2 Dvoryanskaja str., Odesa 65026, Ukraine
e-mail: mnp@onu.edu.ua

K. S. Shakun (✉)
Department of Physics and Chemistry, National University "Odessa Maritime Academy",
8 Didrikhson str., Odesa 65043, Ukraine
e-mail: gluon@meta.ua

L. A. Bulavin and L. Xu (eds.), *Modern Problems of the Physics of Liquid Systems*, Springer Proceedings in Physics 223,
https://doi.org/10.1007/978-3-030-21755-6_2

experiments [10–13]. Therefore, the manifestation of rotational motion in spectra of QEINS is needed in additional study.

The main goal of our work is to investigate the spectral properties of the intermediate scattering function (ISF):

$$F_s(\vec{k}, \omega) = \frac{1}{\pi} \int_0^\infty F_s(\vec{k}, t) \cos \omega t \mathrm{d}t, \tag{2.1}$$

where

$$F_s(\vec{k}, t) = < e^{i\vec{k} \cdot \Delta \vec{r}(t)} >, \tag{2.2}$$

$\Delta \vec{r}(t) = \vec{r}(t) - \vec{r}(0)$ is the displacement of a molecule during time t, $\vec{k}$ is the transferring wave vector. The behavior of $F_s(\vec{k}, t)$ will be modeled with the help of computer simulations. We will consider the peculiarities of the spectral density $F_s(\vec{k}, \omega)$ in the three characteristic cases: (1) $|\vec{k}|a \ll 1$; (2) $|\vec{k}|a \sim 1$ and $|\vec{k}|a \gg 1$, where a is the average interparticle spacing. The special attention will be also focused on the $\vec{k}$-dependence of the half-width $\gamma(\vec{k}^2)$ on the spectral peak on its half-height of the:

$$F_s(\vec{k}, \gamma(\vec{k}^2)) = \frac{1}{2} F_s(\vec{k}, \omega)\Big|_{\omega=0}. \tag{2.3}$$

We will also show that the description of experimental data for the case $|\vec{k}|a \ll 1$ with the help of the diffusion approximation

$$F_s(\vec{k}, \omega) \sim \frac{D_s \vec{k}^2}{\omega^2 + \left(D_s \vec{k}^2\right)^2} \tag{2.4}$$

is quite correct only for $0 < \omega \leq D_s \vec{k}^2$, i.e. the applicability region of the diffusion approximation is strongly restricted. The high-frequency asymptote of $F_s(\vec{k}, \omega)$ for the same values of wave vectors is the more surprising:

$$F_s(\vec{k}, \omega) \sim \exp\left(-(\omega \tau(k))^{2/3}\right), \quad \omega \gg D_s \vec{k}^2, \quad |\vec{k}|a \ll 1, \tag{2.5}$$

i.e. it is radically different from that, $F_s(\vec{k}, \omega) \sim \frac{D_s \vec{k}^2}{\omega^2}$, following from the diffusion approximation.

Comparing the $\vec{k}$-dependence of the half-widths for water and argon for $|\vec{k}|a > 1$ we will be able to establish that the rotational motion of water molecules practically does not influence on characteristic details of $\gamma(\vec{k}^2)$. This result is very important for correct description of the role of molecular rotation.

2.2 Cross-Section for the Quasi-elastic Incoherent Neutron Scattering

In general the displacement $\Delta\vec{r}(t)$ of a molecule can be represented as the sum of two terms

$$\Delta\vec{r}(t) = \Delta\vec{r}^{(\upsilon)}(t) + \Delta\vec{r}^{(d)}(t), \tag{2.6}$$

where the first of them is caused by vibration modes and the latter—by the irreversible thermal drift from the one temporary equilibrium position to another. Since these contributions are statistically independent, the intermediate function (2.2) transforms to the product

$$F_s(\vec{k}, t) \leq \exp(i\vec{k} \cdot \Delta\vec{r}^{(\upsilon)}(t)) > < \exp(i\vec{k} \cdot \Delta\vec{r}^{(d)}(t)) > . \tag{2.7}$$

Since vibration displacements $\Delta\vec{r}^{(\upsilon)}(t))$ are limited: $|\Delta\vec{r}^{(\upsilon)}(t))| < b \ll a$

$$|\vec{k}|b \ll 1 \tag{2.8}$$

we can write:

$$< \exp(i\vec{k} \cdot \Delta\vec{r}^{(\upsilon)}(t)) \geq \exp(-2W), \quad W = \frac{1}{12}\vec{k}^2 < \left(\Delta\vec{r}^{(\upsilon)}(t)\right)^2 >, \tag{2.9}$$

i.e. they generate the standard Debye-Waller factor [1–3].

Now we pass to the consideration of $< \exp(i\vec{k} \cdot \Delta\vec{r}^{(d)}(t)) >$ in the simplest case of the diffusion approximation: $|\vec{k}|a \ll 1$ for argon (Sects. 2.1 and 2.2) and water (Sects. 2.3 and 2.4).

2.2.1 Diffusion Approximation for Argon

In this case translational displacements $\Delta\vec{r}^{(d)}(t)$ of a molecule are described by the distribution function:

$$W\left(\Delta\vec{r}^{d}(t)\right) = \left(\frac{3}{2\pi\Gamma(t)}\right)^{3/2} \exp\left(-3\left(\Delta\vec{r}^{d}(t)\right)^2/(2\Gamma(t))\right), \tag{2.10}$$

which leads together with (2.7) and (2.9) to the result:

$$F_s(\vec{k}, t) = \exp(-2W)\exp\left(-\frac{1}{6}\vec{k}^2\Gamma(t)\right). \tag{2.11}$$

Here $\Gamma(t)$ is the mean square displacement (MSD) of a molecule. In accordance with [14, 15], $\Gamma(t)$ can be represented as the sum:

$$\Gamma(t) = \Gamma_{\mathrm{r}}(t) + \Gamma_{\mathrm{c}}(t), \tag{2.12}$$

where

$$\Gamma_{\mathrm{r}}(t) = 6D_{\mathrm{r}}t + C_{\mathrm{r}} \tag{2.13}$$

is the contribution to the MSD caused by displacements on molecular scales (nanoscales) and

$$\Gamma_{\mathrm{c}}(t) = 6D_{\mathrm{c}}t - B\sqrt{t} + \cdots, \quad B = \frac{k_{\mathrm{B}}T}{\rho(\pi\nu)^{3/2}} \tag{2.14}$$

is caused by the collective transport of molecules in the field of thermal hydrodynamic fluctuations (meso-scales) [14–16]. Here k_{B} is the Boltzmann constant, ρ is the mass density, ν is the kinematic shear viscosity and D_{c} is the collective part of self-diffusion coefficient [16].

It is clear from (2.12)–(2.14) that the Debye-Waller factor takes the form:

$$\exp(-2W) = \exp\left(-\frac{1}{6}\vec{k}^2 C_{\mathrm{r}}\right) \tag{2.15}$$

that allows to estimate $\exp(-2W)$ with the help of computer simulations.

As it had been shown in [15] the collective contribution to the self-diffusion coefficient D_{c} is determined by the expression:

$$D_{\mathrm{c}} = \frac{k_{\mathrm{B}}T}{10\pi\eta\sqrt{\nu\tau_{\mathrm{M}}}}, \tag{2.16}$$

where τ_{M} is the Maxwell relaxation time. The last is determined by the equation:

$$\frac{\partial\vec{u}}{\partial t} + \tau_{\mathrm{M}}\frac{\partial^2\vec{u}}{\partial t^2} = \nu\Delta\vec{u} \tag{2.17}$$

for the transversal hydrodynamic velocity field (see details in [17]).

One can show [18] that the MSD of a molecule can be represented in the form:

$$\Gamma(t) = C_{\mathrm{r}} + 6D_{\mathrm{s}}t\left[1 - \frac{10}{3\pi^{1/2}}\frac{D_{\mathrm{c}}}{D_{\mathrm{s}}}\left(\frac{\tau_{\mathrm{M}}}{t}\right)^{1/2} + \cdots\right], \tag{2.18}$$

where the self-diffusion coefficient D_{s} is the sum of D_{c} and D_{r}:

$$D_{\mathrm{s}} = D_{\mathrm{c}} + D_{\mathrm{r}}. \tag{2.19}$$

If we will use in (2.18) the MSD obtained with the help of computer simulations, we can estimate the relative value of the collective self-diffusion coefficient:

$$\frac{D_c}{D_s} = \frac{3\pi^{1/2}}{10} x^{1/2}\left[1 - \frac{\tilde{\Gamma}(x) - \tilde{c}}{x}\right] + o(1/x^{1/2}), \tag{2.20}$$

where $x = t/\tau_M$, $\tilde{\Gamma}(x) = \Gamma(t)/6D_s\tau_M$ and $\tilde{c} = C_r/6D_s\tau_M$. Since the inequality $x^{1/2} \gg 1$ is consistent with $\tilde{\Gamma}(x) \gg \tilde{c}$, the last equation can be simplified:

$$\frac{D_c}{D_s} = F_{MD}(x), \tag{2.21}$$

where $F_{MD}(x) = \frac{3\pi^{1/2}}{10} x^{1/2}\left[1 - \frac{<\tilde{\Gamma}_{MD}(x)>}{x}\right]$ and $\tilde{\Gamma}_{MD}(x)$ is the MSD determined in computer experiments. The angular brackets in $< \tilde{\Gamma}_{MD}(x) >$ denote the averaging operation on different realizations of $\tilde{\Gamma}_{MD}(x)$ over 6 different initial configurations. Here it is supposed that x satisfies the inequality: $1 \ll x \ll x_u$, where x_u is the upper limit for the applicability of computer simulation modeling. The reliability of such an estimate for the ratio $\frac{D_c}{D_s}$ is naturally verified by its comparison with that calculated as the ratio of D_c given by (2.16) to D_s that is determined experimentally.

Using the Einstein formula for the self-diffusion coefficient: $D_s = \frac{k_B T}{6\pi\eta r_p}$, we can attach the ratio D_c/D_s the following view:

$$\frac{D_c}{D_s} = \frac{3}{5}\frac{r_p}{\sqrt{\nu\tau_M}}, \tag{2.22}$$

where r_p is the effective radius for a molecule.

To find the ratio $\frac{D_c}{D_s}$ according to (2.20) it is necessary to find (1) the time dependence of the MSD and (2) the Maxwell relaxation time.

2.2.2 The Spectrum of the ISF for $|\vec{k}|a \ll 1$

From (2.11) it follows that the spectral density for the ISF is determined by the expression:

$$F_s(\vec{k}, \omega) = \frac{1}{\pi}\exp\left(-\frac{1}{6}\vec{k}^2 C\right)\int_0^\infty \exp\left(-\frac{1}{6}\vec{k}^2\Gamma(t)\right)\cos\omega t\, dt, \tag{2.23}$$

where $\Gamma(t)$ in accordance with (2.12)–(2.14) and (2.19) equals to

$$\Gamma(t) = 6D_s t - B\sqrt{t} + \cdots. \tag{2.24}$$

Since the first term in (2.24) plays the leading role for all $t > t_0$, where $t_0 = \left(\frac{B}{6D_s}\right)^2 \sim 10^{-13}$ s, the spectral density of the ISF can be represented in the form (see [19]):

$$F_s(\vec{k}, \omega) = \exp\left(-\frac{1}{6}\vec{k}^2 C\right)\frac{1}{\pi}\mathrm{Re}\frac{1}{-i\omega + \gamma(\vec{k}^2, \omega)}, \tag{2.25}$$

where the half-width reduces to

$$\gamma(\vec{k}^2, \omega) = D_s\vec{k}^2\left(1 + \gamma_1(\vec{k}^2, \omega)\right) \tag{2.26}$$

and

$$\gamma_1(\vec{k}^2, \omega) = -\frac{b}{2}\sqrt{\pi(1 - i\tilde{\omega})}, \quad \tilde{\omega} = \frac{\omega}{D_s\vec{k}^2}, \quad b = \frac{B}{6\sqrt{D_s}}\left|\vec{k}\right|. \tag{2.27}$$

In low-frequency limit ($\tilde{\omega} \ll 1$) the half width tends to the value:

$$\gamma(\vec{k}^2, \tilde{\omega}) = D_s\vec{k}^2\left(1 - (b/2)\sqrt{\pi}\right), \tag{2.28}$$

i.e. the correction term is proportional to the cubic degree of the wave vector. In the opposite case let us introduce the function:

$$I(\tilde{\omega}, b) = \mathrm{Re}\frac{\tilde{\omega}^2}{-i\tilde{\omega} + 1 + \gamma_1(\vec{k}^2, \tilde{\omega})} - 1, \tag{2.29}$$

having the following high-frequency asymptote:

$$I(\tilde{\omega}, b) \underset{\tilde{\omega}\gg 1}{\Rightarrow} \frac{b}{2\sqrt{2}}\sqrt{\pi\tilde{\omega}}. \tag{2.30}$$

Taking into account the expression (2.27) for b and using the equality $B = \frac{20}{\pi^{1/2}}D_c\sqrt{\tau_M}$, from (2.30) we get:

$$\frac{D_c}{D_s} = R_D(\tilde{\omega}), \tag{2.31}$$

where

$$R_D(\tilde{\omega}) = \frac{6}{5}\left(\frac{2}{\tau_M D_s\vec{k}^2}\right)^{1.2}\frac{I(\tilde{\omega}, b)}{\sqrt{\tilde{\omega}}}. \tag{2.32}$$

Equation (2.31) has the very important value since it allows us to determine in principle the relative value of the collective self-diffusion coefficient using the incoherent neutron scattering data for $\tilde{\omega} \gg 1$.

2.2.3 The Spectrum of the ISF for Water

The thermal motion of molecules in water essentially differ from that in argon due to clusterization effects. Near the triple point of water it can be represented as the vibrational motion during the residence time τ_0 and the consequent movement during time τ_1 to a new temporary equilibrium position. By order of magnitude: $\tau_1 \sim a/\upsilon_T \approx 3 \cdot 10^{-13}$ s, where υ_T is the average value of the thermal velocity of a molecule. If $\tau_1 \ll \tau_0$ it is accepted to say that the thermal motion has the crystal-like character. It is necessary to note that the residence time takes the same order of magnitude as the life time τ_H for an H-bond. In accordance with [20–22] $\tau_H \sim$ several *ps* at the room temperature.

The characteristic change of the ISF is occurred during time $\tau_0 + \tau_1 \approx \tau_0$ therefore we can write:

$$\frac{\partial F_s(\vec{k}, t)}{\partial t} = \frac{1}{\tau_0}\Big(F_s(\vec{k}, t + \tau_0) - F_s(\vec{k}, t)\Big). \tag{2.33}$$

In order to find the difference: $F_s(\vec{k}, t + \tau) - F_s(\vec{k}, t)$ as a function of t, τ_0 and $\vec{k}^2$, let us represent the displacement $\Delta\vec{r}(t)$ of a molecule as the sum:

$$\Delta\vec{r}(t) = \Delta\vec{r}(t_{1,2}) + \Delta\vec{r}(t_{2,3}) + \ldots + \Delta\vec{r}(t_{N-1,N}) \tag{2.34}$$

of consecutive displacements: $\Delta\vec{r}(t_{i-1,i}) = \vec{r}(t_i) - \vec{r}(t_{i-1})$ during τ_0 considered also as a time of an elementary diffusion act. Taking into account that:

$$\Delta\vec{r}(t_{i-1,i}) = \Delta\vec{r}^{(\upsilon)}(t_{i-1,i}) + \Delta\vec{r}^{(d)}(t_{i-1,i}) \tag{2.35}$$

and supposing that displacements $\Delta\vec{r}(t_{i-1,i})$ and $\Delta\vec{r}(t_{j-1,j})$ for $j \neq i$ are statistically independent we obtain for the ISF the following equation:

$$F_s(\vec{k}, t_N) \Rightarrow \exp(-2W) F_d(\vec{k}, t_N), \tag{2.36}$$

where

$$F_d(\vec{k}, t_N) = \Big(f_1(\vec{k}^2)\Big)^N, \quad f_1(\vec{k}^2) = < \exp\Big(i\vec{k} \cdot \Delta\vec{r}^{(d)}(t_{1,2})\Big) > . \tag{2.37}$$

It is not difficult to verify that $F_d(\vec{k}, t_m)$, $1 \leq m \leq N$, satisfies the equation:

$$\left.\frac{\partial F_{\mathrm{d}}(\vec{k},t)}{\partial t}\right|_{t=t_m} = -\frac{1}{\tau_0}F_{\mathrm{d}}(\vec{k},t_m)(1-f_1(\vec{k}^2)), \tag{2.38}$$

which leads to the solution:

$$F_{\mathrm{d}}(\vec{k},t) = \exp\left(-\frac{(1-f_1(\vec{k}^2))}{\tau_0}t\right). \tag{2.39}$$

From (2.36)–(2.39) it follows that the spectral density of the ISF equals to

$$F_{\mathrm{s}}(\vec{k},\omega) = \exp(-2W)\frac{1}{\pi}\frac{\gamma(\vec{k}^2)}{\omega^2+\gamma^2(\vec{k}^2)}, \tag{2.40}$$

where the half-width of the Lorentzian takes the value:

$$\gamma(\vec{k}^2) = \frac{1-f_1(\vec{k}^2)}{\tau_0}. \tag{2.41}$$

To construct the evident view of $f_1(\vec{k}^2)$ we take into account that the shift $\Delta\vec{r}_m^{(d)}$ of a molecule during the time τ_0 can be represented as the sum of two independent contributions:

$$\Delta\vec{r}_m^{(d)} = \Delta\vec{r}_m^{(c)} + \Delta\vec{r}_m^{(r)}, \tag{2.42}$$

where the first of them describes the collective drift of a molecule in the velocity field of thermal hydrodynamic fluctuations and the second—the displacement of a molecule about its nearest neighbors [18, 23]. This displacement has also the collective character and it arises due to small displacements of the nearest neighbors. In other words the first displacements are characterized by meso-scales and the second—by nano-scales. As a result we can write:

$$f_1(\vec{k}^2)) = f_1^{(c)}(\vec{k}^2)\cdot f_1^{(r)}(\vec{k}^2), \tag{2.43}$$

where

$$f_1^{(c)}(\vec{k}^2) = <\exp(i\vec{k}\Delta\vec{r}_m^{(c)})>, \quad f_1^{(r)}(\vec{k}^2) = <\exp(i\vec{k}\Delta\vec{r}_m^{(r)})>. \tag{2.44}$$

In accordance with [14–16, 24] the collective transport is caused by the transversal modes in liquids and it has the diffusion character. Due to this the main contribution to $f_1^{(c)}(\vec{k}^2)$ can be written in the view:

$$f_1^{(c)}(\vec{k}^2) = \exp(-6D_{\mathrm{c}}\vec{k}^2\tau_0), \tag{2.45}$$

where D_c is the collective contribution to the self-diffusion coefficient [14–16].

Writing the function $f_1^{(r)}(\vec{k}^2)$ in the equivalent form:

$$f_1^{(r)}(\vec{k}^2) = \left\langle \frac{\sin k|\Delta\vec{r}_m|}{k|\Delta\vec{r}_m|} \right\rangle \tag{2.46}$$

and averaging $\Delta\vec{r}_m$ by the Gaussian:

$$W(\Delta\vec{r}_m) = \left(\frac{\gamma}{\pi}\right)^{3/2} \exp(-\gamma(\Delta\vec{r}_m)^2), \quad \gamma = \frac{1}{4l_0^2}, \tag{2.47}$$

where l_0 is the typical displacement of a molecule during $\tau_0 + \tau_1 \approx \tau_0$, we get:

$$f_1^{(r)}(\vec{k}^2) = \exp\left(-\vec{k}^2 l_0^2\right). \tag{2.48}$$

In [25] it had been shown that $l_0 \approx a$. Since $|\vec{k}|\, l_0 \sim |\vec{k}|\, a \ll 1$ the function is very close to

$$f_1^{(r)}(\vec{k}^2) \approx \frac{1}{1 + \vec{k}^2 l_0^2} \tag{2.49}$$

characteristic for the model of the jump-like diffusion [22]. Here we should stress that the model of the jump-like self-diffusion is incorrect in water as well as in argon near their triple points since the structural voids in them are absent. Elementary displacements of molecules are mainly caused by circulator motions (see [18]).

The final result for $f_1^{(r)}(\vec{k}^2)$ becomes equal to:

$$\gamma(\vec{k}^2) = \frac{1}{\tau_0}\left(1 - \frac{\exp(-D_c\vec{k}^2\tau_0)}{1 + \tau_0 D_r\vec{k}^2}\right), \tag{2.50}$$

where we use the change $\vec{k}^2 l_0^2 \rightarrow \tau_0 D_r\vec{k}^2$ consistent with our reasons presented above.

This expression is close to that:

$$\gamma_D^{(SS)}(\vec{k}^2) = \frac{1}{\tau_0}\left(1 - \frac{\exp(-2W)}{1 + \tau_0 D_s\vec{k}^2}\right), \tag{2.51}$$

obtained in [8, 26]. However main assumptions made in [8] cannot be justified from the physical point of view.

The applicability region of our results is restricted by the inequality $\tau_0 D_r\vec{k}^2 \ll 1$, or $l_0^2\vec{k}^2 \ll 1$, therefore the half-width (2.50) of the diffusion peak can be expanded in the series:

$$\gamma(\vec{k}^2) \approx D_s\vec{k}^2 - \tau_0 D_r\vec{k}^4 + \tau_0^2 D_r^3\vec{k}^6 + \cdots . \tag{2.52}$$

where $D_s = D_r + D_c$ is the full self-diffusion coefficient.

It is necessary to note, that the representation of $\gamma(\vec{k}^2)$ by the expansion of type (2.52) is only correct from the mathematical point of view. Therefore, the expression for $\gamma(\vec{k}^2)$ in [8] is not quite satisfactory and can be lead to considerable errors.

Thus, remaining within the framework of the diffusion approximation, $a^2\vec{k}^2 \ll 1$ and fitting experimental data for the half-width with the help of (2.52), we can determine the self-diffusion coefficient D_s, its collective part D_r caused by local chaotic displacements and the residence time τ_0. Their temperature dependences are very important especially of the residence time. They had been in details investigated for water in [4, 5, 15]. Values of $D_c = D_s - D_r$ satisfy the inequality $D_c < (\ll) D_s$ that is one of criteria testifying in the favor of the proposed approach.

Here we add that the crystal-like character of thermal motion in water leading to (2.52) is only observed for $T \leq T_H = 315\,\mathrm{K}$. For higher temperatures it becomes inapplicable and the thermal motion in water approaches to argon-like one. Some important details will be presented in the Discussion.

2.3 Modeling of the VACF According to Computer Simulations

In order to construct the VACF for a molecule of argon and water were used the NVT-ensemble including $1 \cdot 10^6$ argon atoms and NVT-ensemble of 512,000 water molecules. In the second case the realistic flexible TIP4P/F water model [27] was used. In a case of argon atoms ensemble particles interacting by means of the Lenard-Jones potential

$$U(r) = 4\varepsilon\left[\left(\frac{\sigma}{r}\right)^{12} - \left(\frac{\sigma}{r}\right)^{6}\right] \tag{2.53}$$

with parameters $\sigma = 0.3409$ nm and $\varepsilon/k_B = 120.04$ K [28].

Molecules in water ensemble interacting via potential:

$$U(r,\theta) = U_{LJ}(r) + U_c(r) + U_{\text{intra}}(r,\theta), \tag{2.54}$$

$$U_{\text{intra}}(r,\theta) = \sum_{i=1,2} d_r\left(1 - \exp\left[-\beta\left(r_{OH_i} - r_0\right)\right]\right)^2 + \frac{1}{2}K_\theta(\theta - \theta_0)^2, \tag{2.55}$$

where $U_{LJ}(r)$—Lenard-Jones contribution, $U_c(r) = kq_1q_2/r^2$—component, that describes coulomb interaction and $U_{\text{intra}}(r,\theta)$—the part describing intramolecular interaction, taking into account the OH length and HOH angle vibrations. Here $\varepsilon/k_B = 93.2$ K, $\sigma = 0.3164$ nm, $q_H = 0.5564e$, $r_0 = 0,0942$ nm, $\beta = 22.8\,\mathrm{nm}^{-1}$, $d_r = 432.6$ kJ/mol, $\theta_0 = 107.4°$, $K_\theta = 367.8\ \mathrm{kJ/(mol\,rad^2)}$ [27].

For all molecular dynamic tasks, the Gromacs 5.13 software environment [29, 30] was used.

The velocity Verlet algorithm for integration of Newton's equations was used. The time step is $4 \cdot 10^{-16}$ s. For Van der Waals and electrostatic interaction calculations the PME method [31] was applied. At the beginning of calculations molecules are arranged within a cell with interparticle spacing corresponding to a considered density. The periodic boundary conditions are applied. The following requirements are carried out in our calculation procedure:

- the cell edge length (l_e) is much greater than the doubled radius (r_I) of the intermolecular interaction ($l_e \gg 2r_I$);
- the characteristic time $\tau_c = l_e/c$, where c is the longitudinal sound velocity, is greater than the simulation time τ_s ($\tau_c > \tau_s$);
- the cut-off distance is $r_I = 9\sigma$;
- the equilibrium value of pressure at given density and temperature is close to the experimental one;
- values of the self-diffusion coefficients obtained from the study of mean square displacement of a molecule and from the expression of the Green-Kubo type are close to each other.

At the initial simulation stage (up to 120 ps), a system is considered as NVE ensemble. After this a system is described as NPT ensemble using the chain of Nose-Hoover thermostats [32, 33] and MTTK barostat [34, 35]. To avoid large oscillations of pressure the high value of "time constant for coupling" [36] is used. As a result, the temperature and pressure of a system are supported to be consistent with their initial values.

The time dependence of the velocity autocorrelation function (VACF) $\phi_V(t) \leq \vec{v}(t)\vec{v}(0) >$ for a molecule is constructed with the help of simulation data on the last stage. Values of the VACF are obtained by averaging over $1.5 \cdot 10^6$ time steps and 6 independent initial configurations. The relative error of MD calculations averaged over $[3 \div 8]$ ps $\varepsilon = 0.168$ (the relative error for two different initial configurations (i and j) is determined as $\varepsilon = 2\,average\left(\frac{|\phi_i(t)-\phi_j(t)|}{|\phi_i(t)+\phi_j(t)|}\right)$. For larger time intervals the relative error significantly increases, for example, $\varepsilon = 0.363$ for $(20 \div 30)$ ps.

The dynamic memory time (τ_d) [37, 38] in our simulation procedure is about 23 ps for argon and 16 ps for water ensemble. For times that are $t > \tau_d$ parasitic noise contributions to the VACF become comparable with useful signal. In order to overcome partially this problem the Savitzky-Golay spline filter [39] is used (the window width takes 80 points).

2.4 The Determination of the MRT

In this Section we consider some general requirements made for the MRT and present a new method for its determination.

2.4.1 General Requirements for the MRT

In this subsection we establish the important inequality for the MRT. We start from the standard Maxwell definition:

$$\tau_{\mathrm{M}} = \eta / G_{\infty}, \tag{2.56}$$

where η is the dynamic shear viscosity and G_{∞} is the high-frequency shear modulus for liquid system. Value of G_{∞} are well known for crystal and amorphous phase of many systems [40]. Therefore the approximate value of the MRT can be estimated as

$$\tau_{\mathrm{M}} = \eta / G_{\mathrm{cr}} \text{ or } \tau_{\mathrm{M}} = \eta / G_{\mathrm{am}}. \tag{2.57}$$

The value for the amorphous phase is preferable since structures of a system in its amorphous and liquid states are closer to each other.

However, the elastic properties of a system essentially change at the melting and consequent its heating that is connected with decrease of the density. The first fact is clearly illustrated on the example of the longitudinal sound velocity c_l for water. In this case, according to [41, 42] near the melting point we have:

$$c_l^{(\mathrm{cr})} = 3.84 \cdot 10^5 \mathrm{cm/s} \text{ and } c_l^{(\mathrm{liq})} \approx 1.4 \cdot 10^5 \text{ cm/s} . \tag{2.58}$$

So noticeable change is also expected for high-frequency transversal sound velocity, although the corresponding estimates for $c_t^{(\mathrm{liq})}$ are absent.

It is evident that (2.57) can be rewritten in the form:

$$\tau_{\mathrm{M}}(T) = \nu(T)/c_t^2(T), \quad c_t^2(T) = G_{\mathrm{am}}/\rho_{\mathrm{am}}, \tag{2.59}$$

where $\nu(T)$ is the kinematic shear viscosity: $\nu(T) = \eta/\rho$. Since the high-frequency transversal and longitudinal sound velocities satisfy the inequality: $c_t < c_{\mathrm{l}}$, we conclude that the MRT should obey the inequality:

$$\tau_{\mathrm{M}} > \nu / c_{\mathrm{l}}^2. \tag{2.60}$$

Comparative values of the MRT for Argon taken from several sources and its lower limit $\tau_{\mathrm{M}}^{(l)} = \nu/c_l^2$ are presented in the Table 2.1.

Unfortunately, only values of the MRT from [45] satisfy to the inequality (2.60). It is clear that such distinctions of numerical values for the MRT reflects defects of methods used for the determination of τ_{M}.

The MRT should also satisfy the second inequality:

$$\zeta(T) > 1, \quad \zeta(T) = 2\sqrt{\nu(T)\tau_{\mathrm{M}}(T)}/\sigma_p, \tag{2.61}$$

Table 2.1 Values of the MRT for liquid Argon on its coexistence curve

T (K)	90	100	110	120	130	140	150
$\tau_M \cdot 10^{13}$ (s) [43]	≈2.28	–	–	–	–	–	–
$\tau_M \cdot 10^{13}$ (s) [44]	1.68	–	1.58	1.57	1.66	1.73	–
$\tau_M \cdot 10^{13}$ (s) [45]	–	–	≈21	≈22	–	–	–
$\tau_M^{(l)} \cdot 10^{13}$ (s)	2.68	2.51	2.45	2.75	3.3	4.85	–

where σ_p is the molecular diameter. Here we take into account that the combination $2\sqrt{\nu\tau_M}$ has meaning of the suitable radius for the Lagrange particle [15, 24]. In other words it is the size of a liquid particle drifting in the fluctuation hydrodynamic velocity field. It is clear that this size should exceed the molecular size and the interparticle spacing having the same order of magnitude.

The characteristic temperature T_*, higher which the MRT loses its meaning, is determined by the equation:

$$\zeta(T_*) = 1. \tag{2.62}$$

2.4.2 MRT for Water

The general view of the VACF for water molecule at $T = 274$ K is presented in the Fig. 2.1.

One can show that (1) the small peak centered at $t_d = 0.15$ ps corresponds to the dimer longitudinal vibrations, only observed for $T < 400$ K; (2) the more large and deep oscillation is genetically connected with elastic transversal and longitudinal

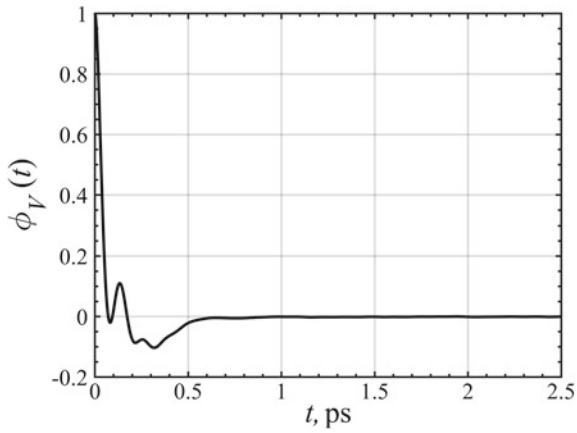

Fig. 2.1 The time dependence of the VACF for a water molecule at 274 K

modes of the hydrodynamic velocity field. This range of negative values for the VACF disappears later, for $T > 450$ K.

In [14, 15, 24] it had been shown that the low-frequency asymptote for the spectral density of the VACF for $T > 450$ K is determined by diffusion transversal modes and it is described by the expression:

$$\phi_{\vec{V}}^{(D)}(\omega) = 3D_c\left[1 - \frac{4}{3}\sqrt{2\pi\omega\tau_M}\left(1 - \frac{3}{2}\omega\tau_M + \frac{3}{8}(\omega\tau_M)^2\right) + \cdots\right]. \tag{2.63}$$

The full correspondence of the last to the VACF-spectrum for $T > 450$ K is demonstrated in the Fig. 2.2.

Near the triple point the important details of the VACF-spectrum are determined by elastic transversal and longitudinal modes. In accordance with [24] their contributions are determined by the formulas:

$$\phi_V(\omega) = \frac{1}{2\pi}\int_0^\infty dt e^{i\omega t}\left(\phi_V^{(t)}(t) + \phi_s^{(l)}(t)\right), \tag{2.64}$$

where

$$\phi_V^{(t)}(t) = \frac{3}{\pi^2}\frac{k_B T}{m_L}\int_0^\infty \frac{du}{u^2}\left(\cos u - \frac{\sin u}{u}\right)^2 \times \left[e^{\frac{t}{2\tau_M}\sqrt{p}} + e^{-\frac{t}{2\tau_M}\sqrt{p}} + \frac{e^{\frac{t}{2\tau_M}\sqrt{p}} - e^{-\frac{t}{2\tau_M}\sqrt{p}}}{\sqrt{p}}\right], \tag{2.65}$$

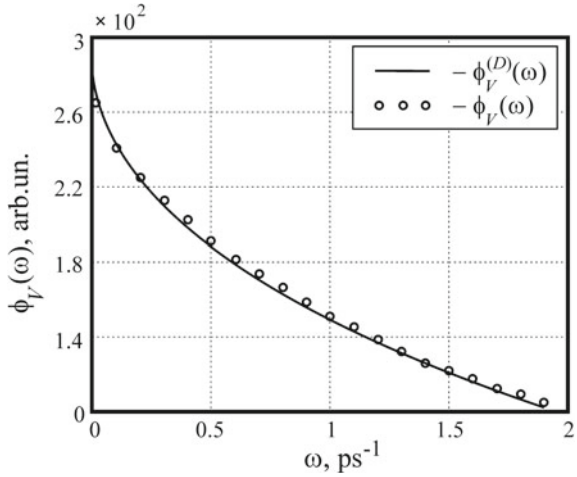

Fig. 2.2 The fitting of the VACF-spectrum (circles) with a help of asymptotic expansion (2.63) at 550 K

$$\phi_s^{(l)}(t) = \frac{3}{\pi}\frac{k_B T}{m_L}\int_0^\infty \frac{du}{u^2}\left(\cos u - \frac{\sin u}{u}\right)^2 e^{-\sigma\theta(u)\,u^2 t/r_L^2}\cos\left(c\frac{u}{r_L}t\right) \tag{2.66}$$

and $p = 1 - u^2$, $r_L = 2\sqrt{\nu\tau_M}$ is the suitable radius of the Lagrange particle (see [15, 24]), $\sigma = \frac{1}{2}\left[\nu + \lambda(\gamma - 1)\right]$, $\lambda = \chi/\rho C_P$, $\gamma = C_P/C_V$, where C_P, C_V are isobaric and isochoric heat capacities and χ is the thermoconductivity coefficient, $\theta(u)$ is the step function.

The comparison of $\phi_V(\omega)$ given by the formulas (2.64)–(2.66) with the VACF-spectrum constructed with the help of MD-simulations is presented in the Fig. 2.3.

Trying for the best fitting of the low frequency part for the VACF-spectrum in the Fig. 2.3 we can determine the MRT for water. Obtained in such a way values of the MRT are gathered in the Table 2.2.

It is necessary to stress here that the values of the MRT satisfying to inequalities (2.60) and (2.62) in fact correspond to that temperature interval where the low-frequency VACF-spectra are determined by quasi-elastic transversal modes.

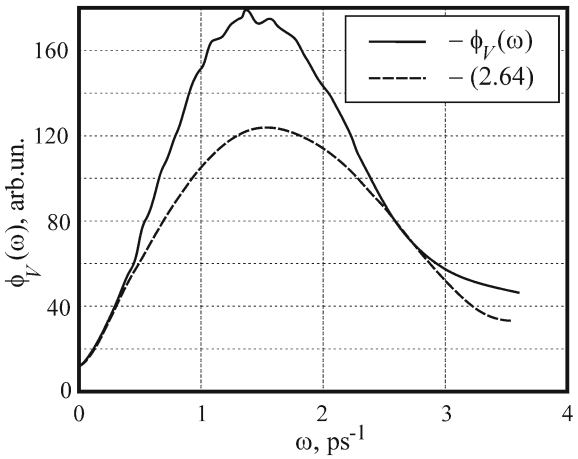

Fig. 2.3 The comparison of the VACF-spectrum (solid line) and that calculated according to (2.64)–(2.66) at 274 K (dashed line)

Table 2.2 Values of τ_M and the right boundary t_{osc} for the VACF oscillation region

P (MPa)	T (K)	τ_M (ps)	t_{osc} (ps)
0.001	274	0.98	1.96
0.0035	300	0.866	1.45
0.042	350	0.612	0.97
0.128	380	0.489	0.744
0.93	450		–

Table 2.3 Values of τ_M, $\zeta(T)$, t_{osc} and D_s for argon as functions of temperature

T (K)	τ_M (ps)	$\zeta(T)$	t_{osc} (ps)	D_s^{MD}(10^{-5}cm^2/s)
85	0.838	2.61	3.08	1.91
90	0.682	2.16	2.28	2.31
100	0.565	1.83	1.48	3.41
110	0.312	1.1	0.64	4.69

2.4.3 The MRT for Argon

In this case all main details of the procedure for the determination of the MRT are the same as for water. Corresponding values of τ_M, $\zeta(T)$, determined by (2.61), t_{osc} and D_s are gathered in the Table 2.3.

As we see from the Table 2.3 the characteristic temperature T_* for argon, determined by (2.60) and (2.62), is close to 110 K. For higher temperatures the MRT for argon loses its physical meaning, i.e. the elastic transversal modes disappear in a system.

2.5 Determination of the Ratio $\frac{D_c}{D_s}$ for Argon and Water

In this section we present results of our investigation of the ratio $\frac{D_c}{D_s}$ for argon and water.

2.5.1 The Ratio $\frac{D_c}{D_s}$ for Argon

In this subsection we present our results of determination of the ratio according to (2.21) and calculated immediately using D_c according to (2.16) and the MRT from the previous Section as well as experimental values for D_s.

Let us consider some details of determination of the ratio $\frac{D_c}{D_s}$ according to (2.21). The averaging of $F_{MD}(x)$ is carried out within time interval: $x_l < x < x_u$, where the lower limit satisfies the inequality: $x_l > 1$ and the upper limit—the one: $x_u < x_d$, where x_d determined by dynamic memory time. The behavior of $F_{MD}(x)$ inside such intervals for several temperatures is presented in the Fig. 2.4.

We see that the plateau in the behavior of $F_{MD}(x)$ is only observed for $T < 120$ K that is consistent with the existence of the MRT namely for these temperatures. Values of the ratio $\frac{D_c}{D_s}$ obtained in such a way are collected in the second column of the Table 2.4. Values of $\frac{D_c}{D_s}$ calculated immediately are placed in the third column.

Thus, the collective part of the self-diffusion coefficient (1) reaches approximately 10% at the triple point of argon; (2) increases with temperature taking its maximal

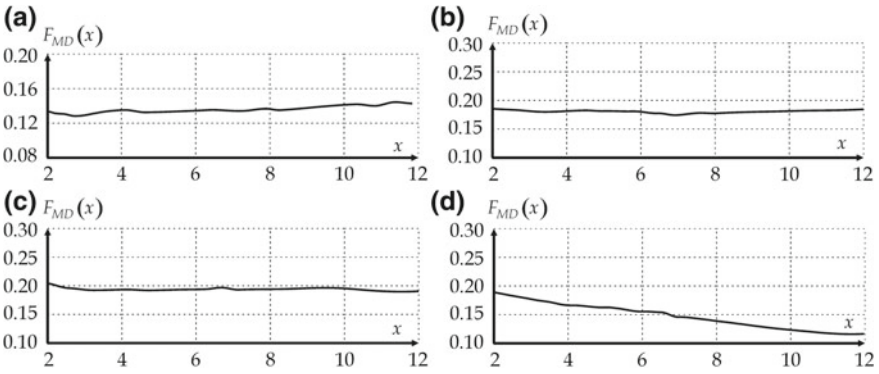

Fig. 2.4 Behavior of $F_{\mathrm{MD}}(x)$ for large enough x at several temperatures: $T = 85$, 100, 110, 120 K (**a**, **b**, **c**, **d** correspondingly)

Table 2.4 Comparative values of the ratio $D_{\mathrm{c}}/D_{\mathrm{s}}$ obtained according to (2.21) and calculated immediately. Experimental values of D_{s} barrowed from [46, 47]

T (K)	$D_{\mathrm{c}}/D_{\mathrm{s}}$ (2.21)	$D_{\mathrm{c}}/D_{\mathrm{s}}$ (immed.)
85	0.138	0.095
90	0.151	0.121
100	0.182	0.166
110	0.192	0.28

value at 110 K (about 25%) and (3) tends to zero with consequent increase of temperature. The last assertion reflects that fact that the MRT for argon becomes its incorrect characteristics for $T > 120$ K. There is a quite satisfactory correlation between values of $D_{\mathrm{c}}/D_{\mathrm{s}}$, obtained according to (2.21) and calculated immediately.

2.5.2 The Ratio $\frac{D_c}{D_s}$ for Water

In the Table 2.5 results of our calculations of D_{s} and $D_{\mathrm{c}}/D_{\mathrm{s}}$ for water are presented. They are obtained with the same procedure as for argon in Sect. 2.5.1.

Table 2.5 Values of D_{s} and $D_{\mathrm{c}}/D_{\mathrm{s}}$ for several temperatures. Experimental values taken from [48, 49]

T (K)	$D_{\mathrm{s}}^{\mathrm{MD}}$	$D_{\mathrm{s}}^{\mathrm{exp}}$	$D_{\mathrm{c}}/D_{\mathrm{s}}$ (2.21)	$D_{\mathrm{c}}/D_{\mathrm{s}}$ (immed)
274	1.529	1.18	0.022	0.036
300	2.779	2.41	0.081	0.076
350	7.04	6.28	0.157	0.133
380	11.07	9.33	0.243	0.182

2.6 MD-Modeling of the Spectrum for the ISF for Argon

In this Section we consider the applicability region of the diffusion approximation for the spectral density of the ISF.

2.6.1 Fitting of Computer Simulation Data with the Help of Diffusion Lorentzians

The behavior of the spectral density for the ISF for Argon in a low-frequency interval $0 < \tilde{\omega} < 3$, where $\tilde{\omega} = \omega/D_s\vec{k}^2$ and $a^2\vec{k}^2 \ll 1$, is presented in the Fig. 2.5.

As we see, (1) the spectral density of the ISF deviates from the Lorentzian already at $\tilde{\omega} \sim 1$ or ($\omega \sim D_s\vec{k}^2$) and (2) the contribution of the root square term in (2.25) is negligibly small, as it should be for small frequencies. The first fact is rather surprising and it should be taken into account at fitting experimental data with the help of Lorentzian. Below we will also give a rigorous theoretical substantiation of the restricted applicability of Lorentzian.

From the Table 2.6 it follows that the optimal fitting of the computer simulation data for the spectrum with the help of Lorentzian is observed for $\tilde{k}_l < \tilde{k} < \tilde{k}_u$ and $0 < \tilde{\omega} < \tilde{\omega}_u$, where the limit values of $\tilde{k}_l$, $\tilde{k}_u$ and $\tilde{\omega}_u$ are depending on density ρ. Speaking about the optimal fitting we suppose that values for the calculated self-diffusion coefficients D_s^{MD} are the closest to corresponding experimental data D_s^{exp}. The density dependence of $\tilde{k}_u$, presented in the Fig. 2.6, is close to the rectilinear one. The values of $\tilde{\omega}_u < 1.7$.

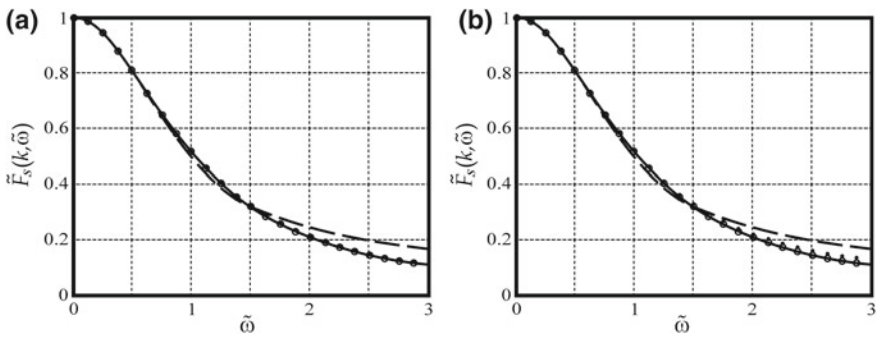

Fig. 2.5 The spectral density of the normalized ISF $\tilde{F}(\vec{k},\tilde{\omega}) = F(\vec{k},\omega)/F(\vec{k},0)$ for argon as a function of frequency $\tilde{\omega}$ at $\rho = 1.0\,\mathrm{g/cm^3}$ and $T = 90\,\mathrm{K}$: dashed line correspond to computer simulation data (CSD); open circles and points are the result of calculation according (2.25) at $b = 0$ and $b = 0.03$ (**a**), as well as $b = 0$ and $b = 0.1$ (**b**); solid curve corresponds to the Lorentzian: $\tilde{F}_{\mathrm{L}}(\vec{k},\tilde{\omega}) = \frac{1}{\tilde{\omega}^2+1}$

Table 2.6 Values of D_s and the upper limit frequency $\tilde{\omega}_u$ for the applicability of Lorentzian for various densities and wave vectors $\tilde{k} = \frac{ak}{2\pi}$ at $T = 135$ K. Experimental values D_s^{exp} taken from [46, 47]

$\rho = 0.8\,g/cm^3$	$\tilde{k}$	0.10	0.22	0.24	0.28
	$D_s^{MD} \cdot 10^5$ (cm/s)	15.7	13.85	12.0	11.2
	$D_s^{exp} \cdot 10^5$ (cm/s)	14.27			
	$\tilde{\omega}_u$	–	1.65	1.5	–
$\rho = 1.0\,g/cm^3$	$\tilde{k}$	0.13	0.214	0.252	0.29
	$D_s^{MD} \cdot 10^5$ (cm/s)	10.61	9.97	8.81	8.3
	$D_s^{exp} \cdot 10^5$ (cm/s)	9.88			
	$\tilde{\omega}_u$	–	1.55	1.4	–
$\rho = 1.2\,g/cm^3$	$\tilde{k}$	0.17	0.26	0.29	0.32
	$D_s^{MD} \cdot 10^5$ (cm/s)	7.76	5.92	5.34	4.9
	$D_s^{exp} \cdot 10^5$ (cm/s)	6.02			
	$\tilde{\omega}_u$	–	1.5	1.3	–
$\rho = 1.4\,g/cm^3$	$\tilde{k}$	0.22	0.27	0.325	0.35
	$D_s^{MD} \cdot 10^5$ (cm/s)	4.71	3.53	3.14	2.88
	$D_s^{exp} \cdot 10^5$ (cm/s)	3.56			
	$\tilde{\omega}_u$	–	1.5	1.3	–

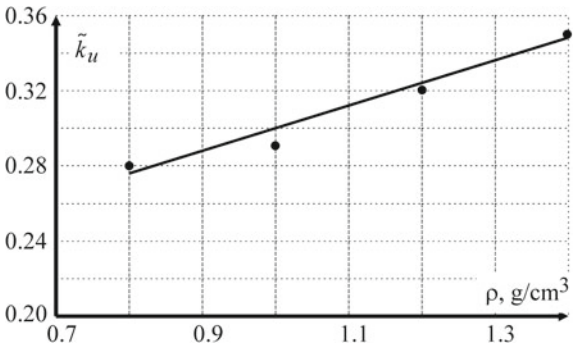

Fig. 2.6 The upper limit for wave vectors as a function of density

As it follows from the Table 2.7, the optimal fitting of experimental data with the help of Lorentzians becomes better for smaller wave vectors. At the same time values of $\tilde{\omega}_u$ a few increase.

Table 2.7 Values of D_s for water and the upper limit frequencies $\tilde{\omega}_u$ for different temperatures. Experimental values of D_s^{exp} barrowed from [48, 49]

$T = 278$ K	$\tilde{k}$	0.15	0.165	0.237	0.316
	$D_s^{MD} \cdot 10^5$ (cm/s)	1.47	1.22	1.17	1.1
	$D_s^{exp} \cdot 10^5$ (cm/s)	1.324			
	$\tilde{\omega}_u$	2.3	1.7	1.5	–
$T = 293$ K	$\tilde{k}$	0.157	0.209	0.25	
	$D_s^{MD} \cdot 10^5$ (cm/s)	2.072	1.864	1.51	
	$D_s^{exp} \cdot 10^5$ (cm/s)	2.02			
	$\tilde{\omega}_u$	2	1.6	–	
$T = 350$ K	$\tilde{k}$	0.073	0.11	0.146	
	$D_s^{MD} \cdot 10^5$ (cm/s)	7.2	5.845	5.5	
	$D_s^{exp} \cdot 10^5$ (cm/s)	6.41			
	$\tilde{\omega}_u$	2.4	1.6	–	

2.6.2 *The Applicability Region of the Diffusion Approximation for Liquids*

In order to establish the value of high frequency limit for description of the ISF spectrum with the help of Lorentzian

$$f_s(\vec{k}, \omega) = \frac{1}{\pi} \frac{\gamma(\vec{k}^2)}{\omega^2 + \gamma^2(\vec{k}^2)} \tag{2.67}$$

let us apply to the inequality:

$$\frac{1}{2} - \frac{1}{1 + \omega^2/\omega_m^2} \leq \frac{1}{m_0} \int_0^{\omega} I_A(\omega')\mathrm{d}\omega' \leq \frac{1}{2}, \quad \omega_m^2 = \frac{m_2}{m_0}, \tag{2.68}$$

having place in the spectral theory of moments [50–52]. Here, $I_A(\omega) \leq A^+(t)A(0) >_\omega$ is the spectrum for the correlation function $< A^+(t)A(0) >$, where the symbol "+" denotes the operation for Hermitian conjugation,

$$m_n = \int_{-\infty}^{\infty} I_A(\omega)\omega^n \mathrm{d}\omega, \quad n = 1, 2, \ldots. \tag{2.69}$$

are the frequency moments for the spectral density $I_A(\omega)$. If $I_A(\omega) \leq A^+(t)A(0) >_\omega$, only even moments are different on zero: $m_{2n} \neq 0$, $m_{2n+1} = 0$. If we will take into account greater number of even moments, the inequality (2.68) becomes more complicated [51, 52]. In accordance with [53, 54]:

$$m_{2n} = < A^{(n)}(t)A^{(n)}(t) >\big|_{t=0}, \tag{2.70}$$

where $A^{(n)}(t)$ is the n-th time derivative from $A(t)$.

In our case $F_s(\vec{k},\omega) = e^{2W}F_d(\vec{k},\omega)$, so $A(t) = \exp(i\vec{k}\vec{r}_d(t))$ and the zero-th frequency moments is equal to

$$m_0 = 1. \tag{2.71}$$

In order to find the second frequency moment let us define the averaged velocity $\dot{\vec{r}}_d(t)$ of a molecule during the time $t_D = 1/D_s\vec{k}^2$ characteristic for the diffusion motion:

$$\dot{\vec{r}}_D(t) = \frac{1}{t_D}\int\limits_{t-t_D/2}^{t+t_D/2} \vec{v}(t')\mathrm{d}t', \tag{2.72}$$

where $\vec{v}(t)$ is the usual velocity of a molecule. From here it follows that the second moment equals to

$$m_2 = < \dot{\vec{r}}_D^{\,2} > \vec{k}^2 \sim 6D_s\vec{k}^2/t_D. \tag{2.73}$$

In accordance with (2.71) and (2.73) the characteristic frequency ω_m takes the value:

$$\omega_m^{(\mathrm{dif})} \sim \sqrt{2}\omega_D,\ \ \omega_D = D_s\vec{k}^2, \tag{2.74}$$

As a result the inequality (2.68) with $I_A(\omega) = F_s(\vec{k},\omega)$ transforms to

$$\frac{1}{2} - \frac{1}{1+(1/2)\tilde{\omega}^2} \le \mathrm{arctg}\,\tilde{\omega} \le \frac{1}{2},\quad \tilde{\omega} = \omega/\omega_D. \tag{2.75}$$

If $\tilde{\omega} \ge 1$ the inequality (2.75) can be simplified:

$$\frac{1}{2} - \frac{1}{1+(1/2)\tilde{\omega}^2} \le \frac{1}{2} - \frac{1}{\pi\tilde{\omega}} + \frac{1}{3\pi\tilde{\omega}^2} + \cdots \le \frac{1}{2}. \tag{2.76}$$

The left inequalities is only correct for frequencies $\tilde{\omega} < \tilde{\omega}_*$ where

$$\tilde{\omega}_* \approx 2 \quad \text{or} \quad \omega_* \approx 2\,\gamma(\vec{k}^2). \tag{2.77}$$

Thus, our analysis allows us to conclude that the fitting of $F_s(\vec{k},\omega)$ by the diffusion Lorentzian (2.67) is satisfactory only for frequencies $\tilde{\omega} < \tilde{\omega}_*$ that is quite consistent with results of the Sect. 2.6.1. This circumstance is necessary to remember at processing of experimental data [55–60].

2.6.3 *Low Frequency Properties of the ISF-Spectrum for Water*

The thermal motion in water is more complicated in comparison with that in argon. In particular, here it is necessary to take into account the rotation of water molecules. At that, from the consideration [10–13] of the dipole relaxation in water it follows that this rotation is close to be quasi-free in the greater part of temperature interval for its liquid states: $0.49T_c < T < T_c$, $T_c = 649$ K.

Only in the narrow interval of liquid states: $0.42T_c < T < 0.49T_c$ and for supercooled ones the orientation correlations become essential. In connection with this we expect that the behavior of kinetic coefficients for water, in particular the self-diffusion coefficient, should noticeably change at $T_H \sim 0.49T_c$. At the same time, the structure of the diffusion peak should remain changeless. The last conclusion is fully supported by the Fig. 2.7.

The wave vector dependence for the half-width of diffusion peaks for water is presented in the Fig. 2.8. It is rectilinear as it should be.

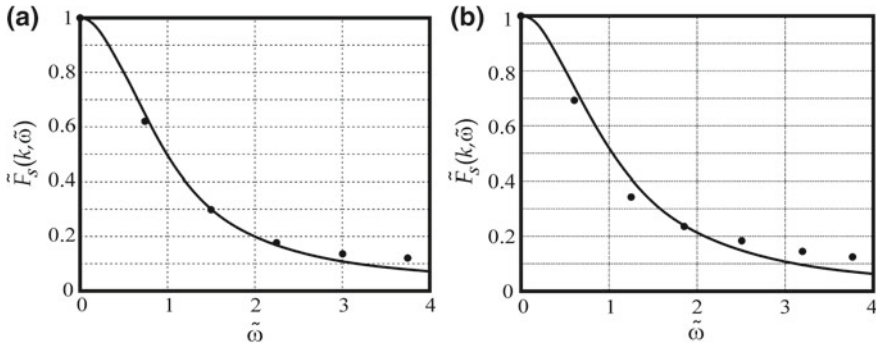

Fig. 2.7 The spectral density $\tilde{F}_s(k, \tilde{\omega})$ of the ISF as a function of $\tilde{\omega}$ at $\rho = 0.997 \mathrm{g/cm}^3$, $T = 293$ K: points correspond to computer simulation data at $\tilde{k} = 0.1$ (**a**) and $\tilde{k} = 0.16$ (**b**), the solid curves correspond to the Lorentzian: $\tilde{F}_L(k, \tilde{\omega}) = \frac{1}{\tilde{\omega}^2+1}$

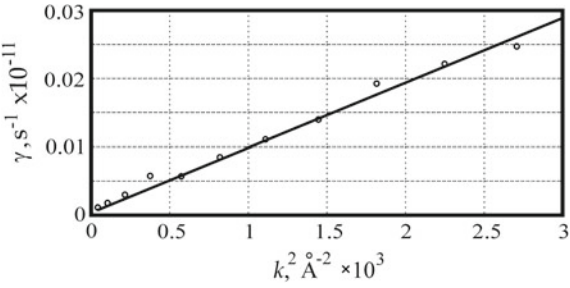

Fig. 2.8 The half-width of the diffusion peak for water as a function of k^2 at $T = 365$ K and small transferring wave vectors: open circles present values of $\gamma(\vec{k}^2)$ obtained with the help of MD-simulations, the solid line corresponds to the equation: $\gamma(\vec{k}^2) = D_s\vec{k}^2$

According to Fig. 2.8 the self-diffusion coefficient of water molecules equals to $D_s = 9.5 \cdot 10^{-5}$ cm^2/s that is close to its experimental value: $D_s = 8.48 \cdot 10^{-5}$ cm^2/s at $T = 365$ K.

Thus the similarity between argon and water spectra as well as the applicability of diffusion Lorentzian for their description is apparent. Therefore, in the following we will focus our attention on the character of wave vector dependence for the half-widths of the incoherent neutron scattering peaks (Fig. 2.9). This question had been experimentally studied in [55–59].

The curves for argon in the Fig. 2.9 correspond to temperatures T_{Ar} and densities n_{Ar} connected with those for water (T_w, n_w) by the similarity relations:

$$T_{Ar} = T_W \frac{T_c^{(Ar)}}{T_c^{(W)}}, \quad n_{Ar} = n_W \frac{n_c^{(Ar)}}{n_c^{(W)}}, \tag{2.78}$$

i.e. computer simulation data are compared for so called corresponding states [61]. Here $T_c^{(Ar)}$, $T_c^{(W)}$ and $n_c^{(Ar)}$, $n_c^{(W)}$ are the critical temperatures and densities for water

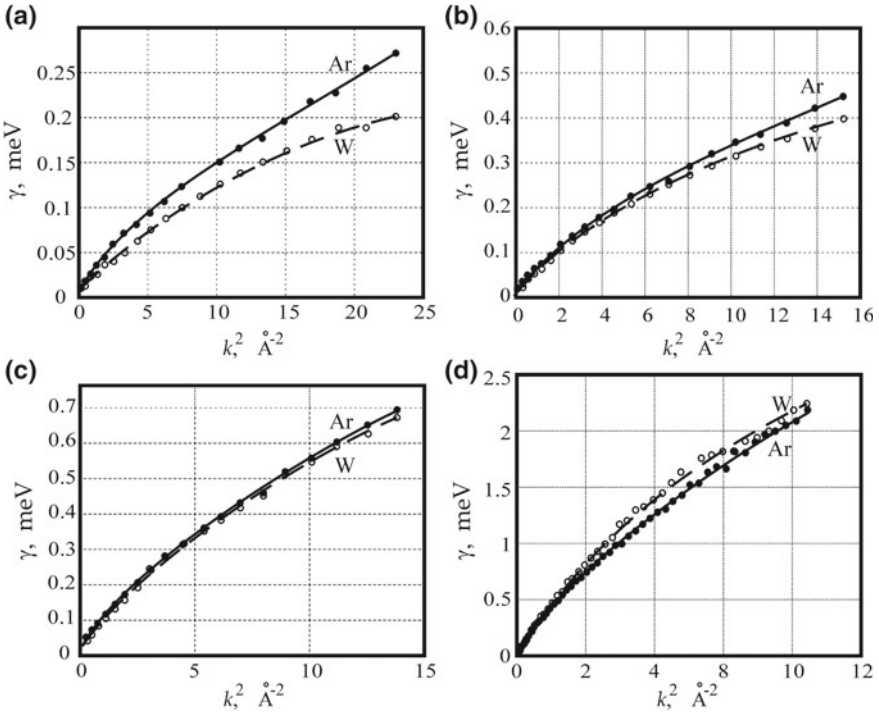

Fig. 2.9 The MD-calculated half-widths of the ISF spectra for water and argon as functions of k^2: open circles and solid lines correspond to argon, dark circles and dashed lines—to water. The curves are constructed at: $T_{Ar} = 59$ K, $T_w = 253$ K—**(a)**, $T_{Ar} = 64.7$ K, $T_w = 278$ K—**(b)**, $T_{Ar} = 68.2$ K, $T_w = 293$ K—**(c)**, $T_{Ar} = 84.5$ K, $T_w = 365$ K—**(d)**

and argon correspondingly. Note, that modeled argon and water remain stable in their supercooled states (see [62]).

Since values of wave vectors in the Fig. 2.9 change in wide limits, including $\tilde{k}^2 \gg (>)1$, shapes of the ISF spectra are very different from Lorentzians. In this case the half-width of peaks are determined by the equation:

$$\tilde{F}_s(\vec{k}, \tilde{\gamma}(\vec{k}^2)) = \frac{1}{2}, \quad \tilde{\gamma}(\vec{k}^2) = \frac{\gamma(\vec{k}^2)}{D_s\vec{k}^2}. \tag{2.79}$$

As we see the half-widths of the ISF peaks for water and argon are practically identical at $T_{Ar} = 68.2\,\mathrm{K}$, $T_w = 298\,\mathrm{K}$, where the last is close to the characteristic temperature $T_H \sim 0.485T_c = 315\,\mathrm{K}$ for water. For temperatures smaller and greater than T_H argon and water curves in Fig. 2.9 differ noticeably from each other. Due to clusterization of water for $T < T_H$ (see [10]) its self-diffusion coefficient additionally diminishes and the water curve in the Fig. 2.9a is shifted down relatively the argon one. If $T > T_H$ the situation is opposite since the self-diffusion coefficient of water is expected to be greater than that in argon. These reasons are also supported by the temperature dependence of the ratio $r_D(T_w) = D_s^{(w)}(T_w)/D_s^{(Ar)}(T_{Ar})$ presented in the Fig. 2.10.

Now we briefly concern an attempt in [3, 55, 56] to explain the $\vec{k}^2$-dependence of the half-width $\gamma(\vec{k}^2)$ for water on the base of hypothesis of rotational motion of molecules. The dotted line in the Fig. 2.11 presents the rotational contribution to the half-width.

It is clear that identical $\vec{k}^2$-dependences for $\gamma_{Ar}(\vec{k}^2)$ and $\gamma_w(\vec{k}^2)$ are not possible to explain assuming that $\vec{k}^2$-dependence of $\gamma_w(\vec{k}^2)$ for water is caused by another mechanism of thermal motion than in argon, in particular, by rotation of water molecules. Moreover, (1) the use of the expression: $\gamma(\vec{k}^2) = \frac{D_s\vec{k}^2}{1+\tau_r D_s\vec{k}^2}$ is incorrect in the diffusion approximation—in this case it is necessary to transform it to the expansion into series with respect to degrees of $\tau_r D_s\vec{k}^2$ similarly to (2.52) and (2) the numerical value of τ_r is too large. Thus, the nonlinear dependence of $\gamma_w(\vec{k}^2)$ on $\vec{k}^2$ is caused by translational motions of water molecules similarly to that in argon.

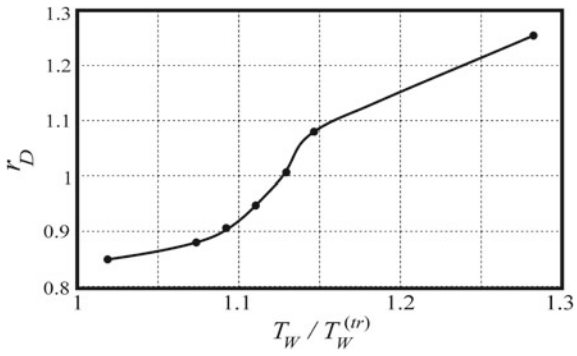

Fig. 2.10 The ratio $r_D(T_w/T_w^{(tr)})$ versus the normalized temperature: $T_w/T_w^{(tr)}$, where $T_w^{(tr)}$ is the temperature for the water triple point. Experimental values of the self-diffusion coefficients for water are taken from [48, 49], argon values are calculated according to the similarity principle

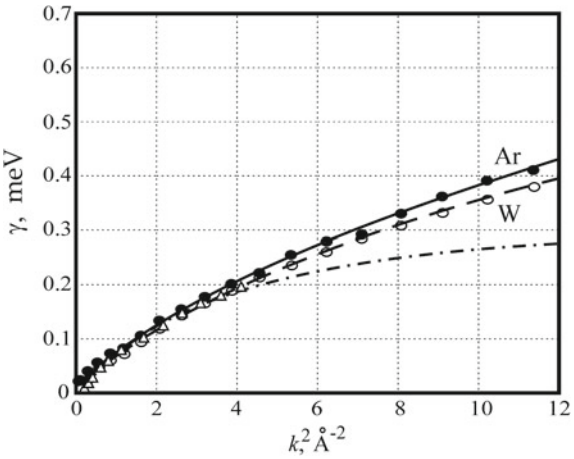

Fig. 2.11 The half-widths of the ISF spectra for water and argon versus $\vec{k}^2$: dark and open circles correspond to $\gamma(\vec{k}^2)$ at $T_{\mathrm{w}} = 278$ K, $T_{\mathrm{Ar}} = 64.7$ K, the solid and dashed curves are fitted with the help of the least-squares method. The dotted line corresponds to $\gamma(\vec{k}^2) = \frac{D_s\vec{k}^2}{1+\tau_r D_s\vec{k}^2}$ with $\tau_{\mathrm{r}} = 2.93 \cdot 10^{-12}$ s, triangles—to experimental data from [55, 56]

Now let us discuss the behavior of the half-width for $1 < \tilde{k}^2 < 10$. As it has been shown in [22] the half-width $\gamma(\tilde{k})$ is a quasi-linear function of the wave vector in this range (see the Fig. 2.12a, b). At that, the ISF is represented by Gaussian: $\tilde{F}(\tilde{k}, \tilde{\omega}) \sim \exp\left(-\tilde{\omega}^2/\gamma^2(\tilde{k})\right)$. As we see, the numerical values of $\gamma(\tilde{k})/\tilde{k}$ on the plateau (b) are close to $3 \cdot 10^4$ cm/s, that coincides with good accuracy with the average thermal velocity of a water molecule: $\upsilon_{\mathrm{T}} \approx 2.91 \cdot 10^4$ cm/s. It means, that main peculiarities of the ISF-spectra in the range: $1 < \tilde{k}^2 < 10$, are caused by quasi-free motion of water molecules. The similar behavior is also expected for argon and argon-like liquids, i.e. having the averaged potentials of argon-like type. As it had

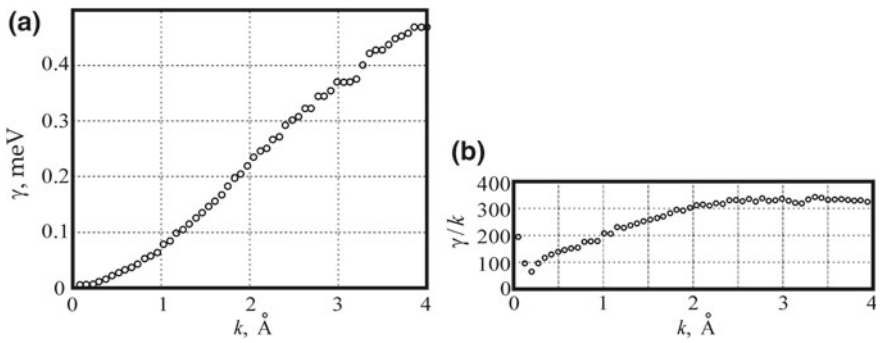

Fig. 2.12 The MD-calculated half-width of the incoherent neutron scattering peak for argon as function of k at $T = 64.7$ K (**a**) and the ratio $\gamma(k)/k$ (**b**)

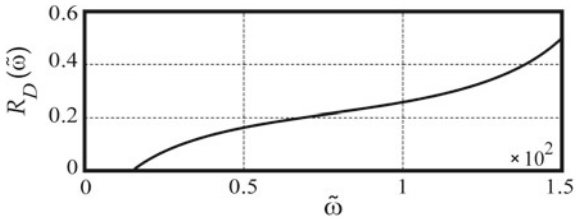

Fig. 2.13 The frequency dependence of $R_D(\tilde{\omega})$ for liquid argon at $k = 0.25\,\text{A}^{-1}$, and $T = 100\,\text{K}$, $\rho = 1.3\ \text{g/cm}^3$

been shown in [63, 64] the majority of low-molecular liquids, including water, belong to this class of similarity.

2.6.4 *Estimate of D_c/D_s for Argon According to Spectral Peculiarities*

In this subsection we will discuss peculiarities of frequency dependence for the ISF spectra at $50 < \tilde{\omega} < 100$ and wave vectors from the diffusion diapason. The behavior of the function $R_D(\tilde{\omega})$ connected with the spectral density of the ISF by the relations (2.30)–(2.32) is presented in the Fig. 2.13.

We see that $R_D(\tilde{\omega})$ monotonously increases although the consideration in the Sect. 2 allowed us to conclude that $R_D(\tilde{\omega})$ should be quasi-constant for $50 < \tilde{\omega} < 100$. In fact, one can say about the point of inflection near $\tilde{\omega}_I \sim 70$, where $R_D(\tilde{\omega}_I) \approx 0.2$. At that, the estimate for D_c/D_s:

$$D_c/D_s \sim R_D(\tilde{\omega}_I) \approx 0.2 \tag{2.80}$$

is quite consistent with that obtained in the Sect. 2.5 from the analysis of the VACF behavior. The absence of plateau in the behavior of $R_D(\tilde{\omega})$ near $\tilde{\omega}_I \sim 70$ is naturally explained by the taking into account of contributions caused by hard collisions between molecules (see details in [65–68]). These contributions, manifested in the ISF spectra, have high-frequency asymptote:

$$F_s(\vec{k}, \omega) \sim \exp\left(-\left(\tau(\vec{k}^2)\omega\right)^{2/3}\right) \tag{2.81}$$

for all wave vectors: $\tilde{k} \ll 1$ and $\tilde{k} \gg 1$ (see Fig. 2.14). The physical nature of this new phenomenon is not fully clear.

2.7 Discussion of the Questions Presented

In the present work we have consider the main peculiarities of the IFS-spectra for water and argon in the applicability region of the diffusion approximation as well as

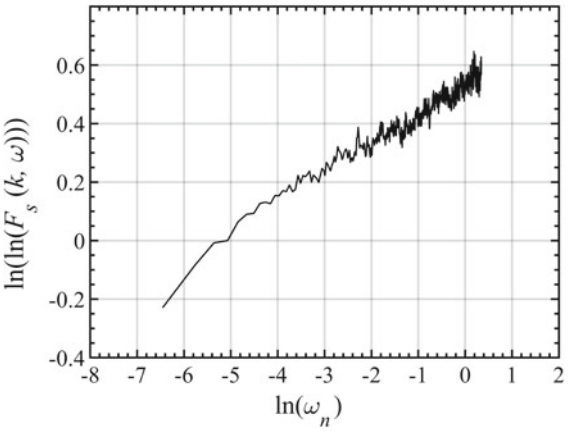

Fig. 2.14 $\ln\ln F_{\rm s}(\vec{k},\omega)$ versus $\ln(\omega_n)$, where $\omega_n = \omega/\omega_{\rm H},\ \omega_{\rm H} = k_{\rm B}T/\hbar$

outside it. At that, the determination of the self-diffusion coefficient $D_{\rm s}$ is regarded by us as well approved.

We have established that the quasi elastic incoherent neutron scattering can be used for the determination of

1. the residence time τ_0 and the collective part $D_{\rm r}$ for the self-diffusion coefficient caused by local displacements of small molecular groups. They can be found from the analysis of $\vec{k}^2$- dependence for the half-width of the diffusion peak (see the formula (2.52));
2. the collective contribution $D_{\rm c}$ to the self-diffusion coefficient caused by molecular drift in the field of velocity hydrodynamic fluctuations according to: $D_{\rm c} = D_{\rm s} - D_{\rm r}$, as well as the ratio $D_{\rm c}/D_{\rm s}$ from the analysis $F_{\rm MD}(x)$ (2.21) and frequency dependence of $R_D(\tilde{\omega})$ (the formula (2.32));
3. applicability region of the MRT. At that, it necessary to take into account that τ_M has only clear physical meaning for temperatures corresponding to the existence of quasi-elastic transversal modes. In fact, such a situation is only realized in a narrow temperature interval adjoining to the triple point of liquids.

It had been also shown that the investigation of the ISF-spectra for $\vec{k}^2a^2 \gg 1$, i.e. outside of the diffusion approximation, give us an important information about $\tau(\vec{k}^2)$ determining the high-frequency asymptotes for $F_{\rm s}(\vec{k},\omega)$. This question is especially important for establishment of peculiarities caused by hard interparticle collisions in molecular systems [65–67].

Using experimental results from [55–57] it had been shown in [4, 5, 15] that the ratio τ_0/τ_f, where $\tau_f \sim a/\upsilon_{\rm T}$, has very surprising temperature dependence (see the Fig. 2.15).

As we see, the inequality $\tau_0/\tau_f > (\gg)1$ takes only place for super-cooled states of ordinary water and its normal ones within the interval:

$$T_m < T < T_{\rm H}, \quad T_m = 273\,{\rm K}, \quad T_{\rm H} \approx 315\,{\rm K}. \tag{2.82}$$

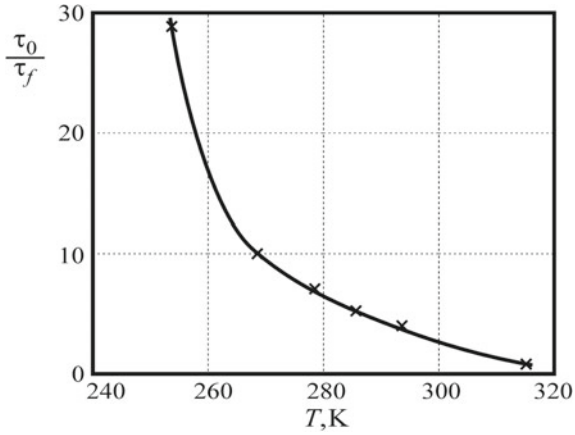

Fig. 2.15 The temperature dependence of the ratio $\frac{\tau_0}{\tau_f}$, where $\tau_f \approx 5 \cdot 10^{-13}$ s

Thus the crystal-like representation for water is only correct for normal and supercooled states corresponding to $T < T_{\mathrm{H}}$. The importance of this result for alive matter is discussed in [69, 70].

It is necessary to stress that our conclusion about the argon-like thermal motion in water for $T > T_{\mathrm{H}}$ is also supported by the temperature dependence of the ratio $\tilde{\tau}_{\mathrm{d}}(t) = \tau_{\mathrm{d}}(t)/\tau_{\mathrm{r}}$, where $\tau_{\mathrm{d}}(t)$ is the dipole relaxation time and τ_{r} is the period of free rotational motion. It is clear that $\tau_{\mathrm{r}} \sim 2\pi/\omega_{\mathrm{T}}$, where $\omega_{\mathrm{T}} \sim \sqrt{k_{\mathrm{B}}T/I}$ is the characteristic value for angular velocity, $I \sim m_{\mathrm{H}} r_{\mathrm{OH}}^2$ is the inertia moment for water molecule (m_{H} is the mass of hydrogen atom and r_{OH} is the distance between hydrogen and oxygen in water molecule). As it had been shown in [71] the nontrivial temperature dependence of $\tilde{\tau}_{\mathrm{d}}(t)$ is only observed for $T < T_{\mathrm{H}}$ (see the Fig. 2.16).

Thus, the quasi-free motion of water molecules is only observed for $T > T_{\mathrm{H}}$ corresponding to destructed crystal-like structure in liquid water.

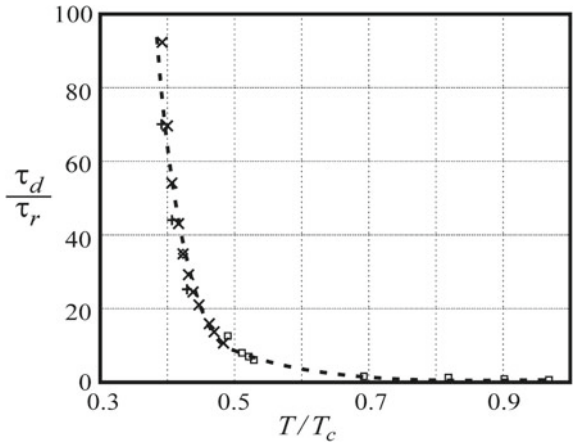

Fig. 2.16 Values of $\tilde{\tau}_{\mathrm{d}}(t)$ as a function of dimensionless temperature: $t = T/T_{\mathrm{c}}$, where T_{c} is the critical temperature. Experimental data are taken from the works: +—[10], □—[11], × —[12], ◊—[13]. The dot line corresponds to exponential dependence

Acknowledgements We cordially thanks Professor S. Magazu, Professor G. G. Malenkov, Professor G. E. Norman, Dr. V. Yu. Bardik and V. Sokolov for fruitfull discussion of our results.

References

1. I.I. Gurevich, L.V. Tarasov, *Low Energy Neutrons Physics* (North-Holland Publishing Co., 1968), p. 621
2. W. Marshall, S.W. Lovesey, *Theory of Thermal Neutron Scattering* (Clarendon Press, Oxford, 1971), p. 620
3. S.-H. Chen, in *Hydrogen-Bonded Liquids*, ed. by J.C. Dore, J. Teixeira (Kluwer Academic Publishers, Netherlands, 1991), p. 289
4. L.A. Bulavin, N.P. Malomuzh, K.N. Pankratov, Character of the thermal motion of water molecules according to the data on quasielastic incoherent scattering of slow neutrons. J. Struct. Chem. **47**, 48–55 (2006). https://doi.org/10.1007/s10947-006-0264-1
5. L.A. Bulavin, N.P. Malomuzh, K.N. Pankratov, Self-diffusion in water. J. Struct. Chem. **47**(Supplement 1), S50–S60 (2006). https://doi.org/10.1007/s10947-006-0377-6
6. J. Frenkel, *Kinetic Theory of Liquids* (Dover Publ, NY, 1955), p. 592
7. E.N. da C. Andrade, The viscosity of liquids. Nature. **125**, 309–310 (1930). http://dx.doi.org/10.1038/125309b0
8. K.S. Singwi, A. Sjolander, Diffusive motions in water and cold neutron scattering. Phys. Rev. **119**, 863–872 (1960). https://doi.org/10.1103/PhysRev.119.863
9. I.L. Fabelinskii, *Molecular Scattering of Light* (Plenum, New York, 1968), p. 622
10. D. Eisenberg, W. Kauzmann, *The Structure and Properties of Water* (Oxford University Press, Oxford, 2005), p. 308
11. K. Okada, M. Yao, Y. Hiejima, H. Kohno, Y. Kojihara, Dielectric relaxation of water and heavy water in the whole fluid phase. J. Chem. Phys. **110**, 3026–3037 (1999). https://doi.org/10.1063/1.477897
12. H.R. Pruppacher, Self-diffusion coefficient of supercooled water. J. Chem. Phys. **56**, 101–108 (1972). https://doi.org/10.1063/1.1676831
13. J.H. Simpson, H.Y. Carr, Diffusion and nuclear spin relaxation in water. Phys. Rev. **111**, 1201–1202 (1958). https://doi.org/10.1103/PhysRev.111.1201
14. T.V. Lokotosh, N.P. Malomuzh, Lagrange theory of thermal hydrodynamic fluctuations and collective diffusion in liquids. Phys. A **286**, 474–488 (2000). https://doi.org/10.1016/S0378-4371(00)00107-2
15. L.A. Bulavin, T.V. Lokotosh, N.P. Malomuzh, Role of the collective self- diffusion in water and other liquids. J. Mol. Liq. **137**, 1–24 (2008). https://doi.org/10.1016/j.molliq.2007.05.003
16. I.Z. Fisher, Gidrodinamicheskaya asimptotika avtokorrelyacionnoy funkcii skorosti molekuli v klassicheskoy zhidkosti (Hydrodynamic asymptotics of the velocity autocorrelation function of a molecule in a classical fluid). JETP (USSR) **61**, 1648–1659 (1971)
17. P.M. Morse, H. Feshbach, *Methods of Theoretical Physics.* Part 1 (McGraw-Hill, NY, 1953) p. 997
18. T.V. Lokotosh, N.P. Malomuzh, K.N. Pankratov, K.S. Shakun, New results in the theory of collective self-diffusion in liquids. Ukr. J. Phys. **60**, 697–707 (2015). http://dx.doi.org/10.15407/ujpe60.08.0697
19. L.A. Bulavin, N.P. Malomuzh, K.S. Shakun, MD-modeling of the intermediate scattering function for argon-like liquids and water. **263**, 200–208 (2018). http://dx.doi.org/10.1016/j.molliq.2018.04.142
20. G.G. Malenkov, Structural and dynamical heterogeneity of stable and metastable water. Phys. A **314**, 477–484 (2002). https://doi.org/10.1016/S0378-4371(02)01085-3

21. V.P. Voloshin, Y. Naberukhin, Hydrogen bond lifetime distributions in computer-simulated water. J. Struct. Chem. **50**, 78–89 (2009). https://doi.org/10.1007/s10947-009-0010-6
22. V.P. Voloshin, Y. Naberukhin, Distributions of hydrogen bond lifetimes in instantaneous and inherent structures of water. Z. Phys. Chem. **223**, 999–1011 (2009). https://doi.org/10.1524/zpch.2009.6062
23. N.P. Malomuzh, Nature of self-diffusion in fluids. Ukr. J. Phys, **63**, 1076–1087 (2018). https://doi.org/10.15407/ujpe63.12.1076
24. T.V. Lokotosh, N.P. Malomuzh, K.S. Shakun, Nature of oscillations for the autocorrelation functions for translational and angular velocities of a molecule. J. Mol. Liq. **96–97**, 245–263 (2002). https://doi.org/10.1016/S0167-7322(01)00351-8
25. T.V. Lokotosh, S. Magazù, G. Maisano, N.P. Malomuzh, Nature of self-diffusion and viscosity in supercooled liquid water. Phys. Rev. E **62**, 3572–3580 (2000). https://doi.org/10.1103/PhysRevE.62.3572
26. P.A. Egelstaff, *An Introduction to the Liquid state* (Academic Press, London, NY, 1967), p. 408
27. M.A. Gonzalez, J.L.F. Abascal, A flexible model for water based on TIP4P/2005. J. Chem. Phys. **135**, 224516(1–8) (2011). http://dx.doi.org/10.1063/1.3663219
28. C. Oostenbrink, A. Villa, A.E. Mark, W.F. van Gunsteren, A biomolecular force field based on the free enthalpy of hydration and solvation: The GROMOS forcefield parameter sets 53A5 and 53A6. J. Comput. Chem. **25**, 1656–1676 (2004). http://dx.doi.org/10.1002/jcc.20090
29. D. van der Spoel, E. Lindahl, B. Hess, G. Groenhof, A.E. Mark, H.J.C. Berendsen, Gromacs: fast, flexible and free. J. Comp. Chem. **26**, 1701–1718 (2005). https://doi.org/10.1002/jcc.20291
30. W.F. van Gunsteren, S.R. Billeter, A.A. Eising, P.H. Hunenberger, P. Kruger, A.E. Mark, W.R.P. Scott, I.G. Tironi, *Biomolecular Simulation: The GROMOS96 Manual and User Guide* (Hochschulverlag AG an der ETH, Zurich, 1996), p. 1044
31. U. Essman, L. Perera, M.L. Berkowitz, T. Darden, H. Lee, L.G. Pedersen, A smooth particle mesh Ewald method. J. Chem. Phys. **103**, 8577–8593 (1995). https://doi.org/10.1063/1.470117
32. S. Nose, A unified formulation of the constant temperature molecular dynamics methods. J. Chem. Phys. **81**, 511–519 (1984). https://doi.org/10.1063/1.447334
33. W.G. Hoover, Canonical dynamics: equilibrium phase-space distributions. Phys. Rev. A **31**, 1695–1697 (1985). https://doi.org/10.1103/PhysRevA.31.1695
34. G.J. Martyna, D.J. Tobias, M.L. Klein, Constant pressure molecular dynamics algorithms. J. Chem. Phys. **101**, 4177–4189 (1994). https://doi.org/10.1063/1.467468
35. G.J. Martyna, M.E. Tuckerman, D.J. Tobias, M.L. Klein, Explicit reversible integrators for extended systems dynamics. Mol. Phys. **87**, 1117–1157 (1996). https://doi.org/10.1080/00268979600100761
36. M.J. Abraham, D. van der Spoel, E. Lindahl, B. Hess, The GROMACS development team, GROMACS User Manual version 2018, www.gromacs.org (2018) 265 p., http://manual.gromacs.org/documentation/2018/manual-2018.pdf. Accessed 12 Dec 2018
37. AYu. Kuksin, I.V. Morozov, G.E. Norman, V.V. Stegailov, I.A. Valuev, Standards for molecular dynamics modelling and simulation of relaxation. Mol. Sim. **31**, 1005–1017 (2005). https://doi.org/10.1080/08927020500375259
38. D. Frenkel, B. Smit, *Understanding Molecular Simulation, Second Edition: From Algorithms to Applications* (Academic Press, San Diego, San Francisco, New York, 2001), p. 664
39. M. Charbit, G. Blanchet, *Digital Signal and Image Processing Using MATLAB* (ISTE Ltd, Telecom ParisTech, 2006), p. 512
40. S. Hess, M. Kroger, W.G. Hoover, Shear modulus of fluids and solids. Phys. A **239**, 449–466 (1997). https://doi.org/10.1016/S0378-4371(97)00045-9
41. C. Vogt, K. Laihem, C. Wiebusch, Speed of sound in bubble-free ice. J. Acoust. Soc. Am. **124**, 3613–8 (2009). https://doi.org/10.1121/1.2996304
42. NIST Standard Reference Database 69: NIST Chemistry WebBook, http://webbook.nist.gov/chemistry/fluid. Accessed 5 Dec 2018
43. A.R. Dexter, A.J. Matheson, Elastic moduli and stress relaxation times in liquid argon. J. Chem. Phys. **54**, 203–208 (1971). https://doi.org/10.1063/1.1674594

44. R. Hartkamp, P.J. Daivis, B.D. Todd, Density dependence of the stress relaxation function of a simple fluid. Phys. Rev. E **87**, 032155 (2013). https://doi.org/10.1103/PhysRevE.87.032155
45. P.S. van der Gulik, The linear pressure dependence of the viscosity at high densities. Phys. A **256**, 39–56 (1998). https://doi.org/10.1016/S0378-4371(98)00197-6
46. R. Laghaei, A.E. Nasrabad, B.C. Eu, Generic van der Waals equation of state, modified free volume theory of diffusion, and viscosity of simple liquids. J. Phys. Chem. B **109**, 5873–5883 (2005). http://dx.doi.org/10.1021/jp0448245
47. B.A. Younglove, H.J.M. Hanley, The viscosity and thermal conductivity coefficients of gaseous and liquid argon. J. Phys. Chem. Ref. Data **15**, 1323–1339 (1986). https://doi.org/10.1063/1.555765
48. R. Mills, Self-diffusion in normal and heavy water in the range 1–45°. J. Phy. Chem. **77**, 685–688 (1973). https://doi.org/10.1021/j100624a025
49. K.R. Harris, L.A. Woolf, Pressure and temperature dependence of the self diffusion coefficient of water and oxygen-18 water. J. Chem. Soc. Faraday Trans. 1. **76**, 377–385 (1980). http://dx.doi.org/10.1039/f19807600377
50. N.I. Akhiezer, M.G. Krein, *Some Questions in the Theory of Moments* (Providence, Amer. Math. Soc., 1962), p. 310
51. M.G. Krein, A.A. Nudelman, *The Markov Moment Problem and Extremal Problems. Translations of Mathematical Monographs*, vol. 50 (Amer. Math. Soc., 1977), p. 417
52. S.J. Karlin, W.J. Studden, *Tchebycheff Systems: With Applications in Analysis and Statistics* (Wiley, London, 1966), p. 586
53. L.D. Landau, E.M. Lifshitz, *Statistical Mechanics* (Pergamon Press, Oxford, 1980), p. 544
54. D. Zubarev, V. Morozov, G. Ropke, *Statistical Mechanics of Nonequilibrium Processes* (Wiley, 1997), p. 376
55. J. Teixeira, M.-C. Bellissent-Funel, S.-H. Chen, J. Dianoux, Experimental determination of the nature of diffusive motions of water molecules at low temperatures. Phys. Rev. A **31**, 1913–1918 (1985). https://doi.org/10.1103/PhysRevA.31.1913
56. J. Teixeira, J.-M. Zanotti, M.-C. Bellissent-Funel, S.-H. Chen, Water in confined geometries. Phys. B **234–236**, 370–374 (1997). https://doi.org/10.1016/S0921-4526(96)00991-X
57. P. Blanckenhagen, Intermolecular vibrations and diffusion in water investigated by scattering of cold neutrons. Ber. Bunsenges. Phys. Chem. **76**, 891–903 (1972). https://doi.org/10.1002/bbpc.19720760907
58. K.-E. Larsson, U. Dahlborg, Proton motion in some hydrogenous liquids studied by cold neutron scattering. Physica **30**, 1561–1599 (1964). https://doi.org/10.1016/0031-8914(64)90181-8
59. G.J. Safford, P.S. Leung, A.W. Naumann, P.C. Schaffer, Investigation of low-frequency motions of H2O molecules in ionic solutions by neutron inelastic scattering. J. Chem. Phys. **50**, 4444–4468 (1969). https://doi.org/10.1063/1.1670917
60. S. Magazu, G. Maisano, F. Migliardo, A. Benedetto, Elastic incoherent neutron scattering on systems of biophysical interest: mean square displacement evaluation from self-distribution function. J. Phys. Chem. **112**, 8936–8942 (2008). https://doi.org/10.1021/jp711930b
61. J.W. Tester, M. Modell, *Thermodynamics and Its Applications,* 3d edn. (Prentice Hall, 1997), p. 960
62. N.P. Malomuzh, K.S. Shakun, Specific properties of argon-like liquids near their spinodals. **235**, 155–162 (2017). https://doi.org/10.1016/j.molliq.2017.01.079
63. S.V. Lishchuk, N.P. Malomuzh, P.V. Makhlaichuk, Why thermodynamic properties of normal and heavy water are similar to those of argon-like liquids? Phys. Lett. A **374**, 2084–2088 (2010). https://doi.org/10.1016/j.physleta.2010.02.070
64. P.V. Makhlaichuk, V.N. Makhlaichuk, N.P. Malomuzh, Nature of the kinematic shear viscosity of low-molecular liquids with averaged potential of Lennard-Jones type. J. Mol. Liq. **225**, 577–584 (2017). https://doi.org/10.1016/j.molliq.2016.11.101
65. V.Yu. Bardic, L.A. Bulavin, V.M. Sysoev, N.P. Malomuzh, K.S. Shakun, in *Soft Matter Under Exogenic Impacts,* ed. by V.A. Mazur, S.J. Rzoska (Springer, 2007), p. 339
66. VYu. Bardic, N.P. Malomuzh, K.S. Shakun, V.M. Sysoev, Modification of an inverse-power potential for simple liquids and gases. J. Mol. Liq. **127**, 96–98 (2006). https://doi.org/10.1016/j.molliq.2006.03.026

67. V.Yu. Bardic, N.P. Malomuzh, V.M. Sysoe, Functional form of the repulsive potential in the high pressure region. J. Mol. Liq. **120**, 27–30 (2005). https://doi.org/10.1016/j.molliq.2004.07.020
68. V.Yu. Bardik, N.P. Malomuzh, K.S. Shakun, High-frequency asymptote for the velocity autocorrelation function spectrum of argon-like systems. J. Chem. Phys. **136**(24), 244511 (2012). http://dx.doi.org/10.1063/1.4729849
69. A.I. Fisenko, N.P. Malomuzh, To what extent is water responsible for the maintenance of the life for warm-blooded organisms? Int. J. Mol. Sci. **10**, 2383–2411 (2009). https://doi.org/10.3390/ijms10052383
70. A.I. Fisenko, N.P. Malomuzh, Role of the H-bond network in the creation of life-giving properties of water. Chem. Phys. **345**, 164–172 (2008). https://doi.org/10.1016/j.chemphys.2007.08.013
71. N.P. Malomuzh, V.N. Makhlaichuk, P.V. Makhlaichuk, K.N. Pankratov, Cluster structure of water in accordance with the data on dielectric permittivity and heat capacity. J. Struct. Chem. **54**, S205–S225 (2013). https://doi.org/10.1134/S0022476613080039